Carbon Trends 7 (2022) 100169

Contents lists available at ScienceDirect

Carbon Trends

journal homepage: www.elsevier.com/locate/cartre

Biocompatible rapid few-layers-graphene synthesis in aqueous lignin solutions

Claudio Marchi[a], Harrison A. Loh[b], Federico Lissandrello[a], Andrea Lucotti[a], Konstantinos A. Sierros[b], Luca Magagnin[a,*]

[a] Dipartimento di Chimica, Materiali e Ingegneria Chimica Giulio Natta, Politecnico di Milano, 20131 Milano, Italy
[b] West Virginia University, Morgantown, West Virginia 26505-3847, United States

ARTICLE INFO

Article history:
Received 6 January 2022
Revised 22 March 2022
Accepted 25 March 2022
Available online xxx

Keywords:
Graphene
Graphite
Liquid Phase Exfoliation
Ultrasounds
Lignin

ABSTRACT

Ultrasonic-Assisted Liquid Phase Exfoliation (UALPE) is considered one of the most promising approaches for the scale-up of graphene production. The process is based on the isolation and stabilization of layers of 2D materials, such as graphene: the selection of a proper stabilizing/exfoliating agent is crucial to achieve a stable Few-Layers-Graphene (FLG) dispersion. In the present work we propose the use of alkali lignin (AL) as a polymeric stabilizing agent for the rapid ($\leq$ 3 hours) synthesis of FLG. Sonication time and graphite-to-lignin (Gr/AL) ratios were investigated as the primary operational parameters to identify the optimal working conditions. Spectroscopical characterization of the samples were employed to assess the quality of the synthesized material: the analysis of the Raman and XPS spectra provided insight on the number of layers and the nature of the limited defects introduced with the exfoliation procedure.

Low-defectivity FLG was obtained at Gr/AL = 8 and a sonication time of 3 hours. Furthermore, Scanning Electron Microscopy and Dynamic Light Scattering were performed to investigate the size of the exfoliated flakes ($\sim$ 400 nm). The procedure proposed represents a rapid route for the synthesis of FLG, which will be further explored for composites in chemiresistive devices.

1. Introduction

Since its discovery, graphene has generated significant interest in the scientific community due to its exceptional chemical, electronic and mechanical properties [1–3]. Despite its appeal, graphene production poses technical challenges related to the desired properties. The quality of graphene is tightly linked to the final application, and, as such, the required synthesis techniques may vary significantly. Typically, bottom-up synthesis routes involve the production of graphene from precursors, such as methane like in chemical vapor deposition (CVD) [4]. However, these vacuum-based techniques are expensive, complex, and generally suitable for more niche uses. Conversely, top-down graphene production, *e.g.,* graphite to graphene, represents a potentially scalable alternative suitable for more widespread applications. The latter sparked much interest in investigating alternative production paths. One of the most promising techniques for the top-down synthesis of graphene is thermal exfoliation. This method is based on exposing a precursor, such as graphite oxide (GO), to high enough temperatures (>550°C) to guarantee the decomposition of the oxygen functional groups [5]. As per Botas et al. [6], such decomposition rate must exceed the diffusion of the gaseous byproducts to overcome graphite's interplanar Van der Waals forces. Despite the requirement for very high temperatures, the simplicity of this method, its scalability, and the absence of toxic chemicals make it a viable top-down approach. Aiming to overcome the strict heating requirements of thermal exfoliation, Lv et al. [7] developed a new production process called "vacuum exfoliation." Briefly, to facilitate the release of oxygen from the starting graphite oxide, a high-vacuum chamber (<1 Pa) was utilized to exfoliate graphene. The added effect of an outward drawing force created by the vacuum allows the thermal exfoliation of graphene at much lower temperatures, as low as 200°C [7]. Due to the high-energy requirements of the abovementioned methods, alternative techniques, such as electrochemical exfoliation, have been developed. Electrochemical exfoliation is based on the intercalation of a graphitic electrode by species dispersed or dissolved in a solution. Alanyalioğlu et al. detail a surfactant-assisted method for synthesizing graphene [8]. The process relies on the electrooxidation of sodium dodecyl sulfate (SDS), leading to its intercalation within the graphite planes. Successively, by applying a negative potential for an extended time (-1V vs. Pt for 2 hours), graphite exfoliation takes place, leading to the synthesis of few-layers-graphene

* Corresponding author.
E-mail address: luca.magagnin@polimi.it (L. Magagnin).

https://doi.org/10.1016/j.cartre.2022.100169

(FLG) [8]. Finally, one of the most relevant and important routes followed is Liquid-Phase Exfoliation (LPE). This process is considerably cheaper and more straightforward than the more common bottom-up vacuum-based methods. LPE is a top-down approach capable of circumventing some of the higher-yielding processes' central issues, such as the chemical reduction of graphene oxide (GO) to reduced graphene oxide (rGO). One critical aspect of GO reduction methods is introducing additional defects in the basal plane of graphene flakes. This occurrence is due to the disruption of the honeycomb-like structure characterized by sp^2 bonds [9]. The presence of defective sites in the graphene flakes gives rise to sp^3 bonded carbon atoms and oxygen-bearing groups that alter the physical properties of the synthesized material. Specifically, the presence of oxygen-bearing carbon atoms in GO and rGO drastically changes the affinity to solvents and overall reactivity of the material: GO, and rGO-based gas sensors show enhanced sensibility due to a more efficient electron transfer thanks to the presence of the defects mentioned above [10,11]. The LPE process consists of overcoming the Van der Walls interlayer forces that bind together graphite layers. The exfoliation mechanism includes mechanical and chemical stimuli that render the inter-planar expansion permanent and stable in suitable solvents.

Specifically, probe (or tip) sonication exfoliation is based on ultrasounds' modulation to control the liquid medium's shear forces and cavitation phenomena. Baig et al. [12] detailed that the former phenomenon affects the ability to separate and isolate graphene layers. The latter is responsible for the creation and sudden collapse of microbubbles, leading to the particles' downsizing and dispersion [12]. Aqueous dispersions of exfoliated graphene are of particular interest due to their low toxicity and biocompatibility. However, water itself is not a "good" solvent for the stabilization of graphene flakes [13,14]. A vast number of stabilizers have been thoroughly evaluated in the literature, such as ionic surfactants, polymeric or aromatic molecules [15]. Green exfoliation routes have quickly gained importance [16–18] and represent one of the more active research fields for graphene. Within the spectrum of biocompatible stabilizers, alkali lignin (AL), traditionally an abundant by-product of the paper industry, is very interesting and highly appealing [19,20]. Its aromatic chemical structure indicates potential π-π stabilization of the graphenic plane, hence a valid candidate for LPE [20]. AL-stabilized graphene's literature is scarce and involves extended production processes (up to 20h) [20–24]. The duration of the sonication process is a crucial aspect in developing a scalable method suitable for the production of larger quantities of graphene. In the present work, we investigate the roles of AL and sonication time in the rapid ultrasonic-assisted LPE (UALPE) of low-defectivity, water-dispersible few-layers-graphene flakes.

2. Materials and methods

Acid-wash graphite flakes from Asbury Carbons were used as the graphite source. The powder was exposed to microwave (MW) irradiation in a standard kitchen microwave DAEWOO KOG-8A07 for 5s cycles to expand the graphitic planes by releasing the intercalated sulfuric and nitric acid. After expansion, the obtained powder was collected and mixed with alkali lignin (low sulfonate content, Sigma-Aldrich) at different weight ratios: 1:1, 2:1, 4:1, 8:1. The dispersion vessel was placed inside an ice bath to avoid excessive heating. Ultra-sonic probe exfoliation was performed with a Toption Ultrasonic Homogenizer TU-900Y at 450W with a 6mm tip with a 50% duty cycle (2′ON/2′OFF). The exfoliation time was varied from 1h to 3h in 30 minutes increments. After transfer to Falcon tubes, the dispersions were centrifuged to isolate the graphene from un-exfoliated graphite particles via step-centrifugation at 50 and 3000 RCFs for 30 minutes using a TOB-TG16G Laboratory centrifuge. Thermal Gravimetric Analysis (TGA) was performed with a PERKIN ELMER STA6000 in air up with a 10°C/min heating rate up to 900°C. TGA was utilized to assess the weight percentage of alkali lignin in the material to calculate the exfoliation efficiency more accurately. The graphene dispersions were centrifuged at 500rpm to remove the unexfoliated material. The precipitate was collected and dried overnight at 70°C on a heating plate before TGA was performed. The weight losses attributed to lignin removal and graphene degradation were used to calculate the fraction of few-layers-graphene (FLG) produced. Raman spectroscopy was used as the primary tool for evaluating the characteristics and quality of the exfoliated graphene. Across the literature, many interpretations have been attributed to the different elements of graphene's Raman spectrum. Nonetheless, its features can be roughly divided into criteria for layers number evaluation and criteria for defectivity analysis. These properties were probed employing graphite to alkali lignin (Gr/AL) ratio and sonication time. To facilitate the observation of the effect of both the exfoliation parameters on Raman spectra, spectroscopical data is presented in the form of heat maps. Raman analysis was performed on five different spots per sample with LABRAM HR 800 UV HORIBA JOBIN YVON on graphene flakes drop casted on a Si/SiO_2 (200nm of oxide) $1 \times 1cm^2$ wafer. Due to AL fluorescence, the analyzed graphene flakes underwent two additional washing steps at 7000 RCF to sediment the material and remove the excess polymer with Millipore water. Laser wavelength was selected at 532nm, with a 50x long focal lens.

X-ray photoelectron spectroscopy (XPS, 25.7 W, 15 kV, monochromated Al Kα X-rays (1488.6 eV) was performed using a PHI 5700 system with an Omni Focus V lens, 100 μm spot size, 45° takeoff angle). XPS analysis was utilized to investigate the chemical nature of the bonds within the samples by performing survey and high-resolution scans for both C1s and O1s spectra. The evolution of carbon and oxygen bonds was probed as a function of the alkali lignin content.

Scanning Electron Microscopy (SEM) for the morphological characterization of graphene flakes was performed on a ZEISS EVO 50 EP. Graphene flakes sedimented after the 7000 RCF centrifugation step were redispersed in H_2O/Ethanol solution and drop casted on Si/SiO_2 $1 \times 1cm^2$ wafer substrates. Ethanol was added to lower the contact angle on the substrates and contrast the coffee ring effect upon evaporating the liquid. ImageJ software was used

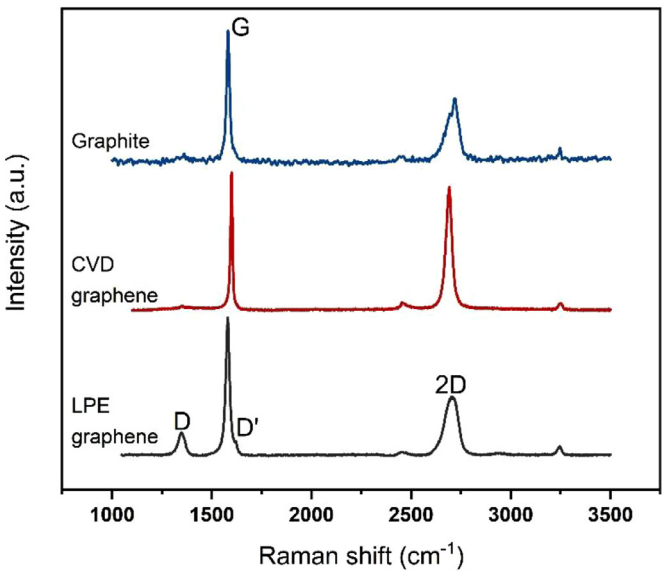

Figure 1. Raman spectra for prisitin graphite (top), commercial CVD graphene (middle), and exfoliated graphene (bottom). The LPE process can be analyzed through Raman data by observation of the main preaks.

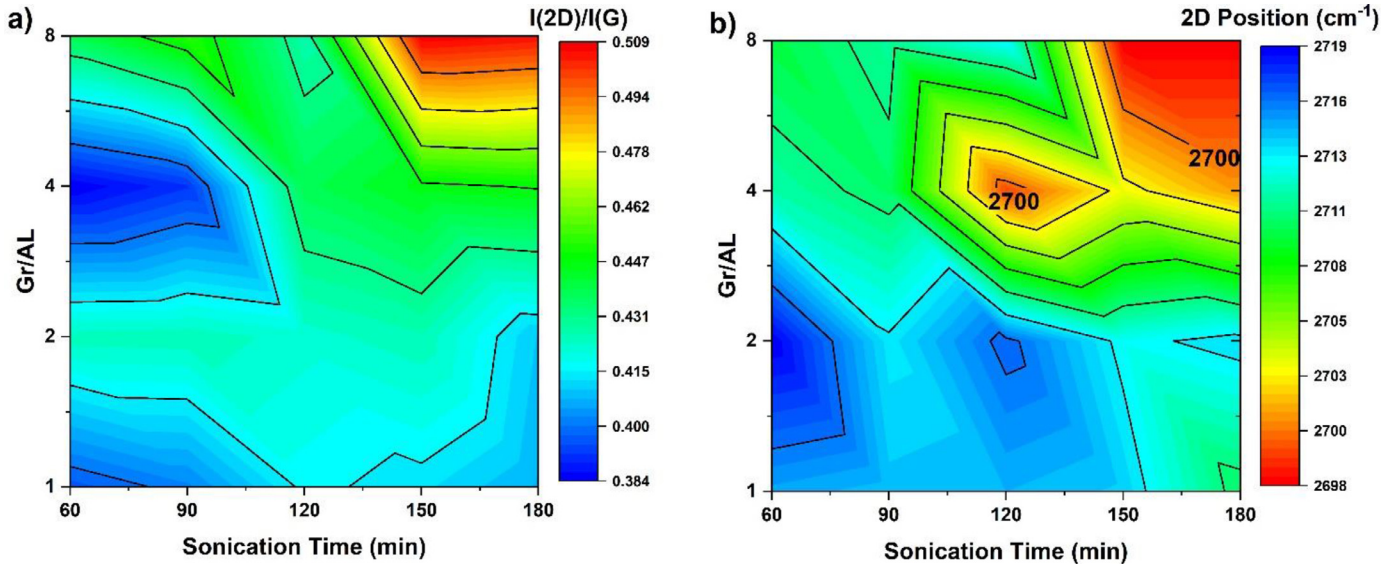

Figure 2. Mapping of Raman data a) I(2D)/I(G) and b) 2D peak position as a function of both sonication time and graphite-to-lignin (Gr/AL) ratio. Increase of the 2D peak intensity (a) and blueshift (b) of the 2D peak position can be observed for higher values of both process parameters.

for the size distribution analysis on the images taken at 10, 20, and 30K magnification. Sixty measurements were performed for every image, providing values for LogNormal distribution fit analysis.

The synthesized graphene flakes were centrifuged at high speed (7000 RCF) and washed twice with 30mL of DIW to remove the alkali lignin excess. The material was redispersed in ethanol and deposited on 300 mesh copper grids coupled with Lacey C films. TEM analysis was performed on a Philips CM200 FEG TEM at 200kV to evaluate the morphology of the exfoliated material. Atomic Force Microscopy (AFM) was performed using an NT-MDT AFM SOLVER PRO in contact mode, mounting a TIPSNANO CSG10 Au coated silicon probe with a force constant of 0.01-0.5 N/m, using a 0.6Hz scan speed. The graphene flakes were drop casted on monocrystalline Si substrates after centrifugation at 7000RCF. Washed and redispersed graphene flakes suspensions in ethanol were utilized for Dynamic Light Scattering (DLS) analysis. The analysis was performed with a Malvern Panalytical Zetasizer Nano after opportune dilution of the graphene dispersions. To cope with the agglomeration and non-spherical nature of the exfoliated material, the monitored variable in the analysis was the position of the primary intensity peak in the DLS spectrum (αPSD).

3. Results and discussion

LPE of graphite into graphene was performed with sonication times within the 3 hours range to accurately evaluate the effectiveness of a promising π-π stabilizer such as alkali lignin in a rapid process (Fig. 1). Liu et al. [20] described the stabilization process in detail by comparing the behavior of both AL-treated and untreated samples. FTIR analysis of the AL-stabilized graphene dispersions shows a shift of the aromatic band vibration, confirming

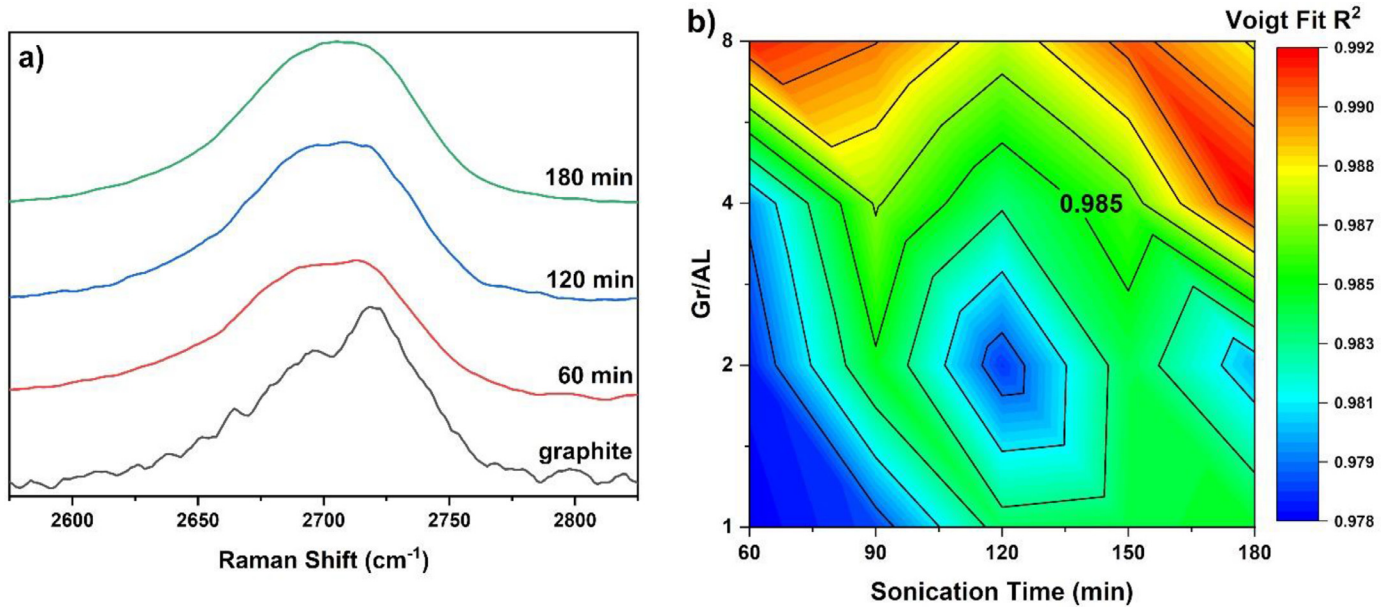

Figure 3. a) Line shape evolution of the 2D peak as a function of sonication time. The increased simmetry of the 2D peak is utilized to evaluate the exfoliation process towards the formation of few-layers-graphene. b) Raman data mapping of R^2 value for the single Voigt curve fit for the 2D peak data.

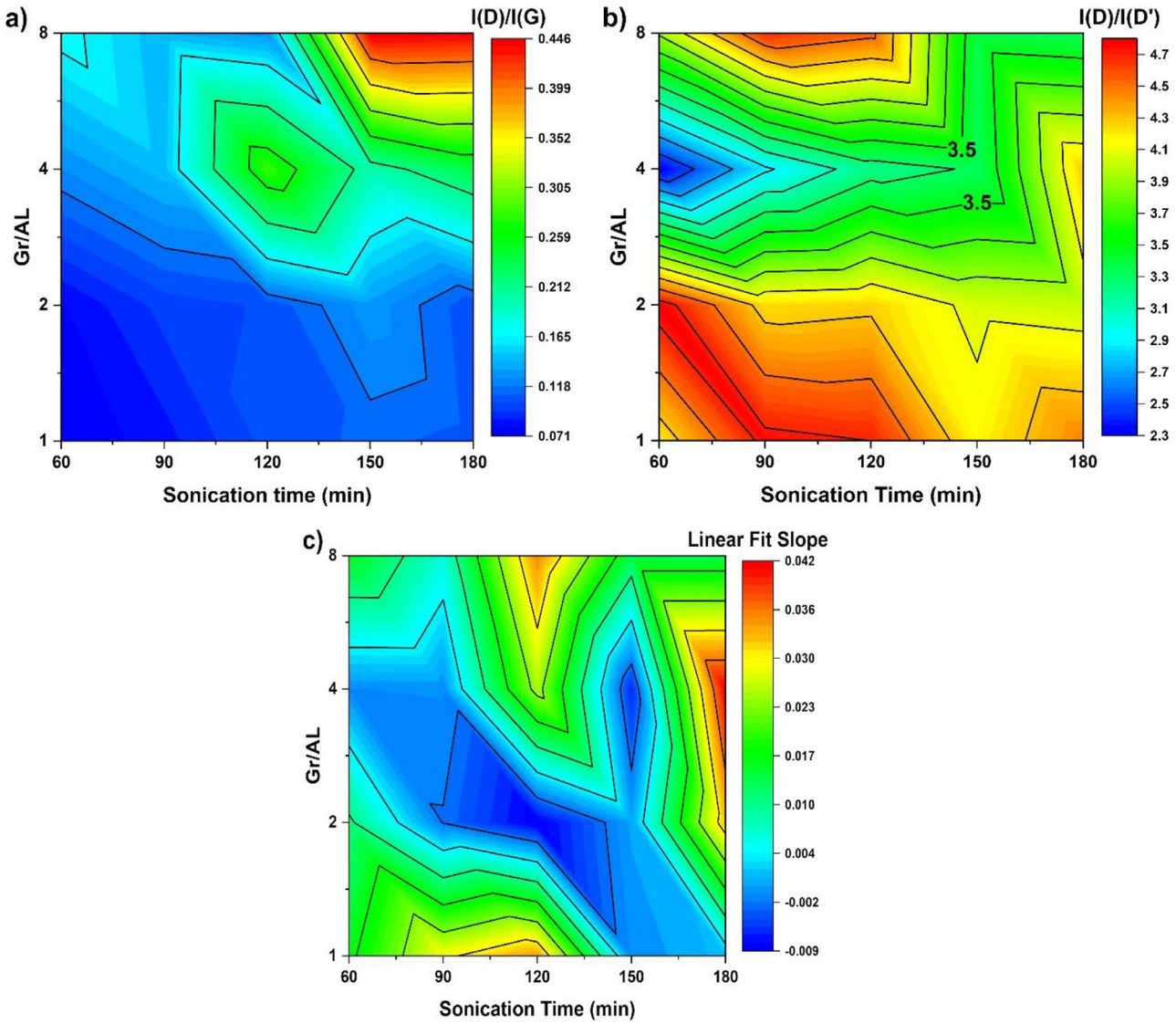

Figure 4. Raman data mapping of a) I(D)/I(G) and b) I(D)/I(D') ratios. Fig. 4c shows the influence of both process parameters on the angular coefficient for the linear fit of I(D)/I(G) vs. FWHM(G).

both the adsorption and the π-π interaction. These findings, coupled with DLS and Z-potential measurements, highlight the ability of lignin to effectively stabilize graphene via electrostatic repulsion (Z-potential value ~ -43mV). Exfoliation efficiency of the LPE process was calculated by weighing the unexfoliated byproduct, *i.e.,* graphite particles removed by 500rpm centrifugation, and analyzed via Thermal Gravimetric Analysis (TGA) to assess the amount of alkali lignin in the material (Fig.S9-12 in Supplementary Information). Efficiency calculations were carried out only for samples graphite-to-lignin Gr/AL=4 and Gr/AL=8 since these conditions were the only ones that resulted in the synthesis of few-layers-graphene (FLG). Specifically, the sample Gr/AL=4 showed a lignin mass loss of 6.74%, resulting in an FLG percentage of 49.88%. On the other hand, the Gr/AL=8 sample shows an FLG fraction of 48.73%, equating to a final concentration of ~1.1 mg/mL for both samples. The assessment of the exfoliation efficiency confirmed the ability of water/alkali lignin to produce FLG dispersions with a final concentration on par with NMP-based systems [15]. Spectroscopical data confirmed how low-defectivity graphene is synthesizable with the proposed rapid process, reaching the 3-5 layers mark, i.e., few-layers- graphene (FLG). Fig. 1 shows the different spectra of graphitic material, the final graphene product, and commercial CVD graphene. Analysis of Fig. 1 spectra shows the evolution of the pristine material via LPE through the insurgence of the D and D' peaks and the evolution of the 2D one.

Analysis of the 2D peak spectrum is widely considered the primary tool for assessing the number of graphene layers via spectroscopical analysis [25–29]. Fig. 2a shows the dependence of the position and intensity of the 2D peak on the UALPE parameters. The analysis highlights a correlation between a blueshift of the 2D peak and increasing Gr/AL and sonication time values. 2700 cm^{-1} was set as the reference point, per literature data showing 2D peaks at lower wavenumbers with decreasing layers [25–29]. The I(2D)/I(G) distribution map (Fig. 2b) shows a similar trend, with more intense 2D peaks associated with higher values of both UALPE parameters. Observation of both maps (Fig. 2a,b) confirms that Gr/AL=8 and t=3h are optimal working conditions. Dependence of the Raman data on Gr/AL ratios for each sonication time interval is highlighted in Fig.S1 in the Supplementary Information (SI). In addition, line shape evaluation and fitting were conducted.

Observation of the shape of the 2D peaks and comparison to related works [25–29] unveils the evolution of the material from a

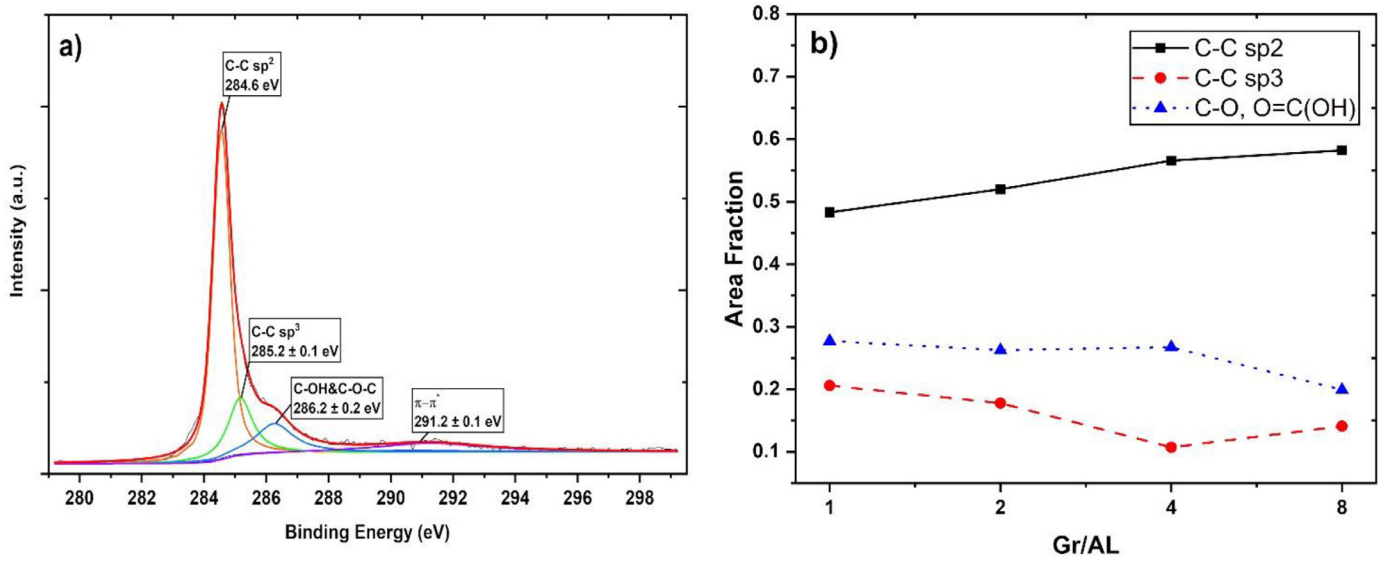

Figure 5. a) XPS high-resolution scan of C1s orbital highlighting the nature of functional groups on the FLG surface. Fig. 5b shows the area fraction of C-C sp2 (continuous line), C-O and O=C(OH) (dotted line), and C-C sp3 (dashed line) as a function of the graphite-to-lignin ratios.

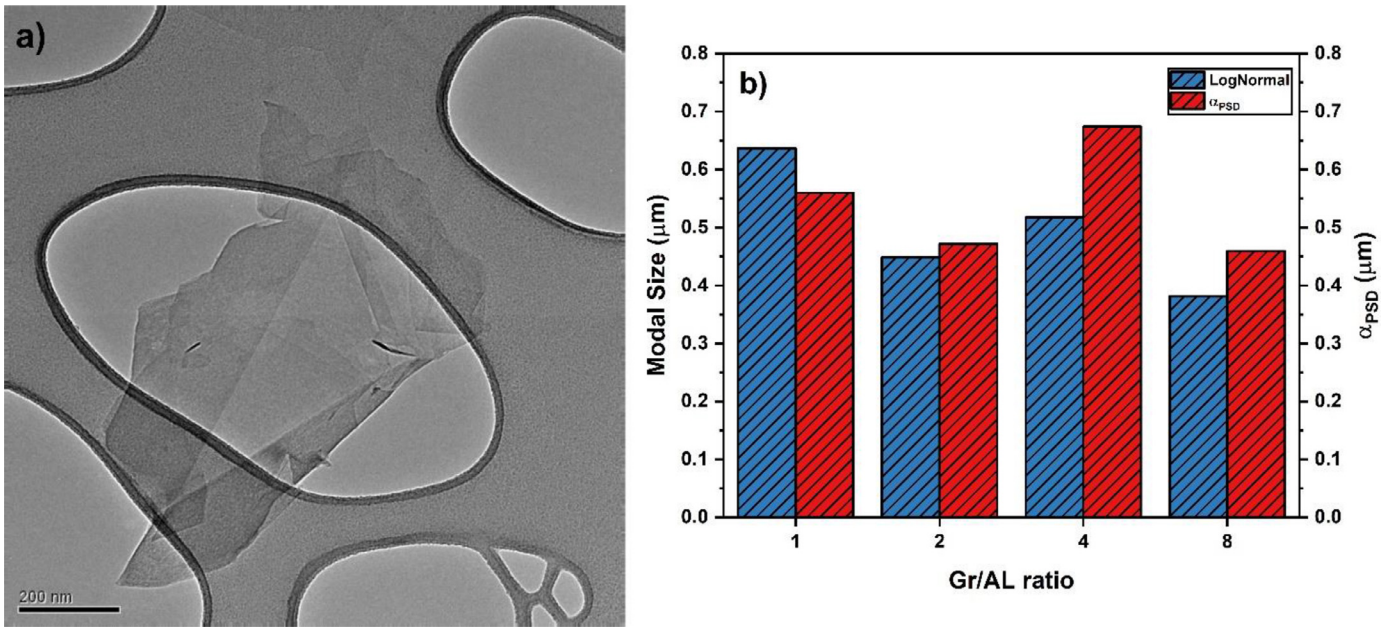

Figure 6. a) TEM image of few-layers-graphene synthesized through the proposed LPE process. Fig. 6b shows the evolution of the modal values (blue) from the LogNormal size distribution analysis performed on SEM images of the synthesized flakes. Data of the primary peak position from DLS analysis on suspended graphene flakes is reported in red.

purely graphitic stage (Fig. 3a) to graphene in the range of 3-5 layers. Further investigation on the 2D peak shape is commonly based on fitting with Lorentzian functions, tuning both the FWHM of said function and the number of curves [27–29]. However, the increasing complexity of the process with a higher number of layers makes an unambiguous interpretation challenging. Roscher et al. [30] suggest using an R^2 value higher than 0.985 for a single Voigt curve fitting as a guideline. Said value consistently correlates to AFM measurements in the original study, confirming the synthesis of few-layers-graphene (FLG). Fig. 3b shows the data map for the R^2 value as a function of both Gr/AL and sonication time, highlighting the beneficial role of lower amounts of lignin and more protracted exfoliation for FLG production. Variations of the R^2 values for the fitting of each time interval are provided in Fig.S2 (SI).

Within graphene's Raman spectrum, the D and D' peaks are commonly correlated to the presence of defects [31–33]. The intensity ratio I(D)/I(G) is proportional to the mean distance between defects [34,35], thus being a good indicator of graphene quality. However, I(D)/I(G) does not provide any information on the nature of those defects. The distinction between bulk and edge defectivity is more easily made by observing the I(D')/I(D) evolution. Eckmann et al. [32] present a guideline to evaluate the type of defects present in graphene. Specifically, when the ratio I(D')/I(D) is roughly 3.5, the contribution to the overall defectivity can be ascribed to the presence of edges. Fig. 4a and 4b show the evolution of both I(D)/I(G) and I(D')/I(D) as functions of UALPE parameters: the significant increase in the I(D)/I(G) value observed for Gr/AL=8 and t=3h corresponds to I(D)/I(D') values (~3.5) indicating the creation of new edges as the dominant phenomenon dur-

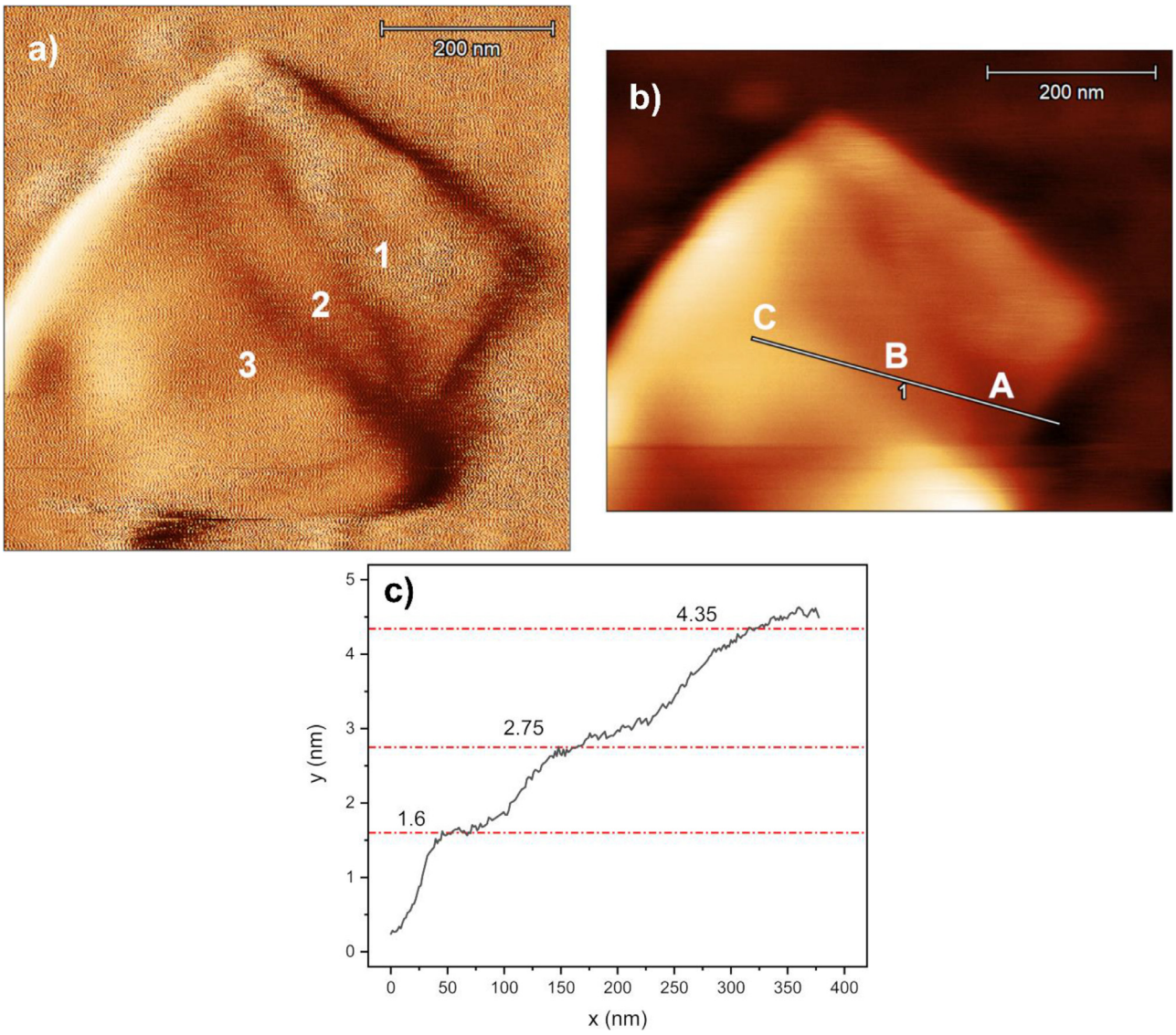

Figure 7. a) Morphology of the wrinkled/folded FLG flake on monocrystalline Si. c) thickness profile of the sample along the measurement line highlighted in b).

ing exfoliation. The dependence of both I(D)/I(G) and I(D)/I(D') on graphite-to-lignin ratios for each sonication time interval is shown in Fig.S3 (SI). The onset of bulk defectivity can also be linked to higher values of FWHM for the G peak [35,36]. In order to further investigate the potential onset of bulk defects caused by the UALPE process, we employed the metric proposed by Bracamonte et al. [37]. Linear fitting of the FWHM(G) vs. I(D)/I(G) values is conducted to extrapolate the degree of correlation between the two variables. The angular coefficient of said fit provides an additional criterion to probe the characteristics of the produced graphene: values closer to 1, i.e., y=x, are representative of a stronger link between sonication time and the presence of basal plane defects. Fig. 4c shows a data map of the evolution of the angular coefficient of the linear fit as a function of Gr/AL and sonication time. The highest value reached within the sample range is 0.042 for Gr/AL ratio equal to 4 and 180 minutes of sonication, corresponding to an angle of 2.4° and highlighting the non-disruptive nature of the exfoliation process, even for the "most damaging" working point. Linear fits for each time window and Gr/AL ratio are shown in SI by Fig.S4-S7.

XPS analysis provided a more in-depth understanding of the influence of AL on the quality of graphene. The testing was conducted on equally sonicated samples for 3hrs, with different Gr/AL ratios: 1,2,4, and 8. Data fitting of the high-resolution scans for C1s and O1s gave insight into the role of the polymeric stabilizer. The prominent peak in the C1s (Fig. 5a) data was attributed to graphene as C-C sp^2 bonds at 284.6 eV, while C-C sp^3 bonds were identified at 285.2 ± 0.1 eV. C-OH and C=O bonds were assigned, respectively, to binding energies (BE) of 285.8 ± 0.1 eV and 286.2 ± 0.1 eV. A broad π-π^* peak linked to HOMO-LUMO transitions can be observed at 290.6 ± 0.5 eV [38–55]. Additionally, a C=O peak at 286.9 ± 0.1 eV and a O=C-OH peak at 289 ± 0.1 eV were present, sporadically, through samples with Gr/AL ratios of 1 to 4. The contribution of sp^2, sp^3 C-C bonds was calculated to investigate AL's role in creating bulk defectivity within the graphene flakes. Fig. 5b highlights the influence of AL concentration on graphene's quality: moving from Gr/AL=1 to Gr/AL=8 leads to a 20% increase in sp^2 C-C, i.e., non-defective graphene. Moreover, Fig. 5b shows the evolution of the oxygen-bearing carbon groups and sp^3 C-C as a function of lignin content: both datasets show a similar decreasing trend, reinforcing the Gr/AL=8 as the optimal working point. XPS data can be correlated to Raman spectroscopy data, thus confirming the non-disruptive nature of AL-stabilized graphene UALPE. The lignin content dependence of sp^3

and sp^2 C-C groups is in agreement with both the FWHM(G) vs. I(D)/(G) fit and I(D)/I(D') Raman data: the higher intensity for the defects-related D peak in the Raman spectra can be attributed to the size reduction of the graphene flakes induced by the ultrasounds, with minimal alteration of the graphenic basal plane structure.

SEM and DLS measurements of the graphene dispersions were utilized to characterize the exfoliated material. However, due to the quasi-2D nature of the graphene flakes, the orientation and state-of-agglomeration of the particles can significantly affect the morphological characterization of FLG. Fig. 6a provides a direct TEM observation of a small packet of folded FLG flakes. Thus, multiple SEM images (Fig.S8 in SI) were taken for each sample and analyzed through a LogNormal distribution fit to account for data variability in the size evaluation process. Dynamic Light Scattering (DLS) of the graphene dispersions was performed to corroborate the interpretation of the SEM data. One critical aspect of DLS analysis for graphene is the non-spherical nature of the material. The estimated hydrodynamic radius is obtained from the Stokes-Einstein equation assuming a spherical particle [56]. Hence, according to Lotya et al. analysis on exfoliated 2D materials size evaluation [57], instead of considering the Z-average value, a better metric for non-polarized DLS analysis is the α_{PSD} value, *i.e.*, the primary intensity peak position in the DLS spectrum. Modal values were considered more relevant than mean values for the analysis, given the influence of agglomerates on calculating the average size. Fig. 6b shows the calculated sizes for both SEM and DLS analysis, highlighting a size range of 400-600 nm without a clear dependence on the alkali lignin concentration. The Gr/AL ratio 8 provides the smallest flakes, 380 nm (SEM) and 460 nm (DLS), substantiating the interpretation of new edges formation as the primary source of the detected defectivity in the Raman spectra.

Spectroscopical data analysis and interpretation lead to identifying the optimal exfoliation conditions, *i.e.,* graphite-to-lignin mass ratio (Gr/AL) equal to 8 and sonication time of 3 hours. In order to further confirm the ability of the proposed method to synthesize Few-Layers-Graphene (FLG), Atomic Force Microscopy (AFM) was employed. AFM imaging was used to analyze the synthesized material's morphology and size. Fig. 7a shows a partially folded graphene flake made of three distinct strata. The thickness evolution associated with the stacked layers is shown in Fig. 7b and Fig. 7c: along the measurement line, it is possible to distinguish individual strata's thicknesses $\leq$1.6nm, thus identifying the overall particle's size at <5nm. AFM data was found to be in agreement with the spectroscopical analysis of the exfoliated material, confirming the synthesis of Few-Layers-Graphene (FLG).

4. Conclusions

The combination of alkali lignin and sonication time in the rapid liquid-phase exfoliation can be used to produce graphene from graphite, exploiting the π-π interaction capability of AL in producing and stabilizing aqueous dispersions of few-layers-graphene. Spectroscopical data highlight the influence of both AL, as biocompatible stabilizer, and sonication time on the final product. Higher graphite-to-lignin ratios (4 and 8) showed the best results in terms of exfoliation effectiveness (3-5 layers of graphene), as confirmed by AFM analysis, and low-defectivity (I(D)/I(D')$\sim$3.5). These results confirm the hypothesis that a limited sonication time ($\leq$ 3hrs) represents a valid route to achieve the synthesis of few-layers-graphene. Further developments of the process will focus on the functionalization of the produced FLG as the active material for electrochemical and chemiresistive gas sensing applications.

Declaration of competing interest

The authors declare that they have no known competing financial interests or personal relationships that could have appeared to influence the work reported in this paper.

Supplementary materials

Supplementary material associated with this article can be found, in the online version, at doi:10.1016/j.cartre.2022.100169.

References

[1] T. Torres, Graphene chemistry, Chem. Soc. Rev. 46 (2017) 4385–4386, doi:10.1039/c7cs90061a.
[2] K.S. Novoselov, V.I. Fal'Ko, L. Colombo, P.R. Gellert, M.G. Schwab, K. Kim, A roadmap for graphene, Nature 490 (2012) 192–200, doi:10.1038/nature11458.
[3] D.G. Papageorgiou, I.A. Kinloch, R.J. Young, Mechanical properties of graphene and graphene-based nanocomposites, Prog. Mater. Sci. 90 (2017) 75–127, doi:10.1016/j.pmatsci.2017.07.004.
[4] Y. Zhang, L. Zhang, C. Zhou, Review of chemical vapor deposition of graphene and related applications, Acc. Chem. Res. 46 (2013) 2329–2339, doi:10.1021/ar300203n.
[5] M.J. McAllister, J.L. Li, D.H. Adamson, H.C. Schniepp, A.A. Abdala, J. Liu, M. Herrera-Alonso, D.L. Milius, R. Car, R.K. Prud'homme, I.A. Aksay, Single sheet functionalized graphene by oxidation and thermal expansion of graphite, Chem. Mater. 19 (2007) 4396–4404, doi:10.1021/CM0630800.
[6] C. Botas, P. Álvarez, C. Blanco, R. Santamaría, M. Granda, M.D. Gutiérrez, F. Rodríguez-Reinoso, R. Menéndez, Critical temperatures in the synthesis of graphene-like materials by thermal exfoliation-reduction of graphite oxide, Carbon N. Y. 52 (2013) 476–485, doi:10.1016/j.carbon.2012.09.059.
[7] W. Lv, D.-M. Tang, Y.-B. He, C.-H. You, Z.-Q. Shi, X.-C. Chen, C.-M. Chen, P.-X. Hou, C. Liu, Q.-H. Yang, Low-temperature exfoliated Graphenes: vacuum-promoted exfoliation and electrochemical energy storage, ACS Nano 3 (2009) 3730–3736, doi:10.1021/nn900933u.
[8] M. Alanyalioğlu, J.J. Segura, J. Oró-Sol, N. Casañ-Pastor, The synthesis of graphene sheets with controlled thickness and order using surfactant-assisted electrochemical processes, Carbon N. Y. (2012) 142–152 Pergamon, doi:10.1016/j.carbon.2011.07.064.
[9] M. Cheng, R. Yang, L. Zhang, Z. Shi, W. Yang, D. Wang, G. Xie, D. Shi, G. Zhang, Restoration of graphene from graphene oxide by defect repair, Carbon N. Y. 50 (2012) 2581–2587, doi:10.1016/J.CARBON.2012.02.016.
[10] S. Yang, C. Jiang, S. Wei, Gas sensing in 2D materials, Appl. Phys. Rev. 4 (2017) 021304, doi:10.1063/1.4983310.
[11] J.T. Robinson, F.K. Perkins, E.S. Snow, Z. Wei, P.E. Sheehan, Reduced graphene oxide molecular sensors, Nano Lett 8 (2008) 3137–3140, doi:10.1021/NL8013007.
[12] Z. Baig, O. Mamat, M. Mustapha, A. Mumtaz, K.S. Munir, M. Sarfraz, Investigation of tip sonication effects on structural quality of graphene nanoplatelets (GNPs) for superior solvent dispersion, Ultrason. Sonochem. 45 (2018) 133–149, doi:10.1016/J.ULTSONCH.2018.03.007.
[13] Y. Hernandez, M. Lotya, D. Rickard, S.D. Bergin, J.N. Coleman, Measurement of multicomponent solubility parameters for graphene facilitates solvent discovery, Langmuir 26 (2010) 3208–3213, doi:10.1021/la903188a.
[14] J.N. Coleman, Liquid exfoliation of defect-free graphene, Acc. Chem. Res. 46 (2013) 14–22, doi:10.1021/ar300009f.
[15] Y. Xu, H. Cao, Y. Xue, B. Li, W. Cai, Liquid-phase exfoliation of graphene: an overview on exfoliation media, techniques, and challenges, Nanomaterials 8 (2018) 942, doi:10.3390/nano8110942.
[16] V.J. González, A.M. Rodríguez, V. León, J. Frontiñán-Rubio, J.L.G. Fierro, M. Durán-Prado, A.B. Muñoz-García, M. Pavone, E. Vázquez, Sweet graphene: Exfoliation of graphite and preparation of glucose-graphene cocrystals through mechanochemical treatments, Green Chem 20 (2018) 3581–3592, doi:10.1039/c8gc01162a.
[17] M. Yi, Z. Shen, S. Ma, X. Zhang, A mixed-solvent strategy for facile and green preparation of graphene by liquid-phase exfoliation of graphite, J. Nanoparticle Res. 14 (2012) 1–9, doi:10.1007/s11051-012-1003-5.
[18] S. Zhao, S. Xie, Z. Zhao, J. Zhang, L. Li, Z. Xin, Green and high-efficiency production of graphene by tannic acid-assisted exfoliation of graphite in water, ACS Sustain. Chem. Eng. 6 (2018) 7652–7661, doi:10.1021/ACSSUSCHEMENG.8B00497.
[19] M.A. Saiful Badri, M.M. Salleh, N.F. ain Md Noor, M.Y.A. Rahman, A.A. Umar, Green synthesis of few-layered graphene from aqueous processed graphite exfoliation for graphene thin film preparation, Mater. Chem. Phys. 193 (2017) 212–219, doi:10.1016/j.matchemphys.2017.02.029.
[20] W. Liu, R. Zhou, D. Zhou, G. Ding, J.M. Soah, C.Y. Yue, X. Lu, Lignin-assisted direct exfoliation of graphite to graphene in aqueous media and its application in polymer composites, Carbon N. Y. 83 (2015) 188–197, doi:10.1016/j.carbon.2014.11.036.
[21] S. Wang, Z. Hu, J. Shi, G. Chen, Q. Zhang, Z. Weng, K. Wu, M. Lu, Green synthesis of graphene with the assistance of modified lignin and its application in anticorrosive waterborne epoxy coatings, Appl. Surf. Sci. 484 (2019) 759–770, doi:10.1016/j.apsusc.2019.03.229.

[22] M.A. Saiful Badri, M.M. Salleh, N.F. ain Md Noor, M.Y.A. Rahman, A.A. Umar, Green synthesis of few-layered graphene from aqueous processed graphite exfoliation for graphene thin film preparation, Mater. Chem. Phys. 193 (2017) 212–219, doi:10.1016/j.matchemphys.2017.02.029.
[23] M.A.S. Badri, N.F.M. Noor, A.R.M. Zain, M. MatSalleh, T.H.T.A. Aziz, Exfoliated graphene-alkaline lignin-PEDOT: PSS composite as a transparent conductive electrode:, https://Doi.Org/10.1177/18479804211015009. 11 (2021). doi:10.1177/18479804211015009.
[24] S.I.S. Shahabadi, J. Kong, X. Lu, Aqueous-only, green route to self-healable, UV-resistant, and electrically conductive polyurethane/graphene/lignin nanocomposite coatings, acs sustain. chem. eng. 5 (2017) 3148–3157, doi:10.1021/acssuschemeng.6b02941.
[25] A.C. Ferrari, J.C. Meyer, V. Scardaci, C. Casiraghi, M. Lazzeri, F. Mauri, S. Piscanec, D. Jiang, K.S. Novoselov, S. Roth, A.K. Geim, Raman spectrum of graphene and graphene layers, Phys. Rev. Lett. 97 (2006), doi:10.1103/PhysRevLett.97.187401.
[26] D. Yoon, H. Moon, H. Cheong, J. Choi, J. Choi, B. Park, Variations in the raman spectrum as a function of the number of graphene layers, J. Korean Phys. Soc. 55 (2009) 1299–1303, doi:10.3938/JKPS.55.1299.
[27] Z. Ni, Y. Wang, T. Yu, Z. Shen, Raman spectroscopy and imaging of graphene, Nano Res 1 (2008) 273–291, doi:10.1007/s12274-008-8036-1.
[28] L.M. Malard, M.A. Pimenta, G. Dresselhaus, M.S. Dresselhaus, Raman spectroscopy in graphene, Phys. Rep. 473 (2009) 51–87, doi:10.1016/J.PHYSREP.2009.02.003.
[29] G.S. Papanai, I. Sharma, B.K. Gupta, Probing number of layers and quality assessment of mechanically exfoliated graphene via Raman fingerprint, Mater. Today Commun. 22 (2020) 100795, doi:10.1016/J.MTCOMM.2019.100795.
[30] S. Roscher, R. Hoffmann, O. Ambacher, Determination of the graphene–graphite ratio of graphene powder by Raman 2D band symmetry analysis, Anal. Methods. 11 (2019) 1224–1228, doi:10.1039/C8AY02619J.
[31] C. Backes, K.R. Paton, D. Hanlon, S. Yuan, M.I. Katsnelson, J. Houston, R.J. Smith, D. McCloskey, J.F. Donegan, J.N. Coleman, Spectroscopic metrics allow in situ measurement of mean size and thickness of liquid-exfoliated few-layer graphene nanosheets, Nanoscale 8 (2016) 4311–4323, doi:10.1039/c5nr08047a.
[32] A. Eckmann, A. Felten, A. Mishchenko, L. Britnell, R. Krupke, K.S. Novoselov, C. Casiraghi, Probing the nature of defects in graphene by Raman spectroscopy, Nano Lett 12 (2012) 3925–3930, doi:10.1021/nl300901a.
[33] R. Beams, L.G. Cançado, L. Novotny, Raman characterization of defects and dopants in graphene, J. Phys. Condens. Matter. 27 (2015) 083002, doi:10.1088/0953-8984/27/8/083002.
[34] A.C. Ferrari, J. Robertson, Interpretation of Raman spectra of disordered and amorphous carbon, Phys. Rev. B. 61 (2000) 14095, doi:10.1103/PhysRevB.61.14095.
[35] L.G. Cançado, A. Jorio, E.H.M. Ferreira, F. Stavale, C.A. Achete, R.B. Capaz, M.V.O. Moutinho, A. Lombardo, T.S. Kulmala, A.C. Ferrari, Quantifying defects in graphene via raman spectroscopy at different excitation energies, Nano Lett 11 (2011) 3190–3196, doi:10.1021/NL201432G.
[36] C. Casiraghi, A. Hartschuh, H. Qian, S. Piscanec, C. Georgi, A. Fasoli, K.S. Novoselov, D.M. Basko, A.C. Ferrari, Raman spectroscopy of graphene edges, Nano Lett. 9 (2009) 1433–1441, doi:10.1021/NL8032697.
[37] M.V. Bracamonte, G.I. Lacconi, S.E. Urreta, L.E.F. Foa Torres, On the nature of defects in liquid-phase exfoliated graphene, J. Phys. Chem. C. 118 (2014) 15455–15459, doi:10.1021/jp501930a.
[38] M.P. Araújo, O.S.G.P. Soares, A.J.S. Fernandes, M.F.R. Pereira, C. Freire, Tuning the surface chemistry of graphene flakes: new strategies for selective oxidation, RSC Adv 7 (2017) 14290–14301, doi:10.1039/C6RA28868E.
[39] J.H. Choi, J. Lee, M. Byeon, T.E. Hong, H. Park, C.Y. Lee, Graphene-based gas sensors with high sensitivity and minimal sensor-to-sensor variation, ACS Appl. Nano Mater. 3 (2020) 2257–2265, doi:10.1021/ACSANM.9B02378.
[40] L. Dong, Z. Chen, X. Zhao, J. Ma, S. Lin, M. Li, Y. Bao, L. Chu, K. Leng, H. Lu, K.P. Loh, A non-dispersion strategy for large-scale production of ultra-high concentration graphene slurries in water, Nat. Commun. 91 (2017) 1–8 9 (2018, doi:10.1038/s41467-017-02580-3.
[41] J. Ederer, P. Janoš, P. Ecorchard, J. Tolasz, V. Štengl, H. Beneš, M. Perchacz, O. Pop-Georgievski, Determination of amino groups on functionalized graphene oxide for polyurethane nanomaterials: XPS quantitation vs. functional speciation, RSC Adv 7 (2017) 12464–12473, doi:10.1039/C6RA28745J.
[42] R. Ghosh, A. Singh, S. Santra, S.K. Ray, A. Chandra, P.K. Guha, Highly sensitive large-area multi-layered graphene-based flexible ammonia sensor, Sensors Actuators B Chem 205 (2014) 67–73, doi:10.1016/J.SNB.2014.08.044.
[43] L. Guardia, M.J. Fernández-Merino, J.I. Paredes, P. Solís-Fernández, S. Villar-Rodil, A. Martínez-Alonso, J.M.D. Tascón, High-throughput production of pristine graphene in an aqueous dispersion assisted by non-ionic surfactants, Carbon N. Y. 49 (2011) 1653–1662, doi:10.1016/J.CARBON.2010.12.049.
[44] P. Kamedulski, A. Ilnicka, J.P. Lukaszewicz, M. Skorupska, Highly effective three-dimensional functionalization of graphite to graphene by wet chemical exfoliation methods, Adsorpt 25 (2019) 631–638 2019 253, doi:10.1007/S10450-019-00067-9.
[45] F. Liu, F. Niu, T. Chen, J. Han, Z. Liu, W. Yang, Y. Xu, J. Liu, One-step electrochemical strategy for in-situ synthesis of S,N-codoped graphene as metal-free catalyst for oxygen reduction reaction, Carbon N. Y. 134 (2018) 316–325, doi:10.1016/J.CARBON.2018.04.007.
[46] Z. Lu, G. Chen, W. Hao, G. Sun, Z. Li, Mechanism of UV-assisted TiO2/reduced graphene oxide composites with variable photodegradation of methyl orange, RSC Adv 5 (2015) 72916–72922, doi:10.1039/C5RA11814J.
[47] S.T. Mitchell, N. Frese, A. Gölzhäuser, A. Bowers, K. Sattler, Ultralight carbon nanofoam from naphtalene-mediated hydrothermal sucrose carbonization, Carbon N. Y. 95 (2015) 434–441, doi:10.1016/J.CARBON.2015.08.001.
[48] M.A. Kang, S. Ji, S. Kim, C.Y. Park, S. Myung, W. Song, S.S. Lee, J. Lim, K.S. An, Highly sensitive and wearable gas sensors consisting of chemically functionalized graphene oxide assembled on cotton yarn, RSC Adv 8 (2018), doi:10.1039/c8ra01184b.
[49] F. Priante, M. Salim, L. Ottaviano, F. Perrozzi, XPS study of graphene oxide reduction induced by (100) and (111)-oriented Si substrates, Nanotechnology 29 (2018) 075704, doi:10.1088/1361-6528/AAA320.
[50] K.S. Rao, J. Senthilnathan, Y.-F. Liu, M. Yoshimura, Role of peroxide ions in formation of graphene Nanosheets by electrochemical exfoliation of graphite, Sci. Reports 4 (2014) 1–6 2014 41, doi:10.1038/srep04237.
[51] V. Strong, S. Dubin, M.F. El-Kady, A. Lech, Y. Wang, B.H. Weiller, R.B. Kaner, Patterning and electronic tuning of laser scribed graphene for flexible all-carbon devices, ACS Nano 6 (2012) 1395–1403, doi:10.1021/NN204200W.
[52] Y. Su, S. Jia, J. Du, J. Yuan, C. Liu, W. Ren, H. Cheng, Direct writing of graphene patterns and devices on graphene oxide films by inkjet reduction, Nano Res 8 (2015) 3954–3962 2015 812, doi:10.1007/S12274-015-0897-5.
[53] S. Tian, S. Yang, T. Huang, J. Sun, H. Wang, X. Pu, L. Tian, P. He, G. Ding, X. Xie, One-step fast electrochemical fabrication of water-dispersible graphene, Carbon N. Y. 111 (2017) 617–621, doi:10.1016/J.CARBON.2016.10.044.
[54] G. Wang, Z. Wang, Z. Liu, J. Xue, G. Xin, Q. Yu, J. Lian, M.Y. Chen, Annealed graphene sheets decorated with silver nanoparticles for inkjet printing, Chem. Eng. J. 260 (2015) 582–589, doi:10.1016/J.CEJ.2014.09.037.
[55] Q. Zhang, F. Zhang, S.P. Medarametla, H. Li, C. Zhou, D. Lin, 3D printing of graphene aerogels, Small 12 (2016) 1702–1708, doi:10.1002/SMLL.201503524.
[56] J. Amaro-Gahete, A. Benítez, R. Otero, D. Esquivel, C. Jiménez-Sanchidrián, J. Morales, Á. Caballero, F.J. Romero-Salguero, A comparative study of particle size distribution of graphene Nanosheets synthesized by an ultrasound-assisted method, Nanomaterials 9 (2019), doi:10.3390/NANO9020152.
[57] M. Lotya, A. Rakovich, J.F. Donegan, J.N. Coleman, Measuring the lateral size of liquid-exfoliated nanosheets with dynamic light scattering, Nanotechnology 24 (2013) 265703, doi:10.1088/0957-4484/24/26/265703.